

The structure of a *Xanthomonas* general stress protein involved in citrus canker reveals its flavin-binding property

Eduardo Hilario, Yang Li, Dimitri Niks and Li Fan*

Department of Biochemistry, University of California-Riverside, Riverside, California, USA

Correspondence e-mail: lifan@ucr.edu

Xanthomonas citri pv. *citri* (*Xac*) causes citrus canker and affects citrus agriculture worldwide. Functional genetic analysis has indicated that a putative general stress protein (XacGSP) encoded by the Xac2369 gene is involved in the bacterial infection. In this report, the crystal structure of XacGSP was determined to 2.5 Å resolution. There are four XacGSP molecules in the crystal asymmetric unit. Each XacGSP monomer folds into a six-stranded antiparallel β -barrel flanked by five α -helices. A C-terminal extension protrudes from the sixth β -strand of the β -barrel and pairs with its counterpart from another monomer to form a bridge between the two subunits of an XacGSP dimer. Two XacGSP dimers cross over each other to form a tetramer; the β -barrels from one dimer contact the β -barrels of the other, while the two bridges are distant from each other and do not make contacts. The three-dimensional structure of the XacGSP monomer is very similar to those of pyridoxine 5-phosphate oxidases, a group of enzymes that use flavin mononucleotide (FMN) as a cofactor. Consistent with this, purified XacGSP protein binds to both FMN and flavin adenine dinucleotide (FAD), suggesting that XacGSP may help the bacteria to react against the oxidative stress induced by the defense mechanisms of the plant.

Received 22 February 2012

Accepted 31 March 2012

PDB References: XacGSP, 3u34; 3u35.

1. Introduction

Xanthomonas is a large genus of Gram-negative bacteria comprising 27 species that collectively cause infectious diseases in about 400 plant hosts, including many economically important crops such as rice and citrus. For example, *X. citri* pv. *citri* (*Xac*) is a widespread phytopathogen and causes the most severe form of citrus canker, known as bacterial canker type A. Citrus canker has been found in all types of citrus trees, causing blemished fruit, premature leaves, fruit abscission, die-back of twigs and general debilitation of the tree. The disease is widespread in many tropical and subtropical areas, causing significant economic losses in citrus production worldwide (Civerolo, 1984; Cubero *et al.*, 2001; Graham *et al.*, 2004). There are no chemical or microbiological agents to control citrus canker; the only efficient control is the removal of infected twigs and the eradication of sick trees from the production areas (Laia *et al.*, 2009). Improvements in bacterial plant-disease control and prevention require a better understanding of the pathogenesis of *Xanthomonas* bacteria.

Recent results obtained from functional and comparative genomic studies provide insights into how *Xanthomonas*

bacteria have adapted to exploit an extraordinary diversity of plant hosts. To date, the complete genome sequences of more than ten *Xanthomonas* strains, including *Xac*, have been determined (Ryan *et al.*, 2011). *Xac* strain 306 bacteria contain a circular genomic DNA and two plasmids (da Silva *et al.*, 2002) encoding 4313 open reading frames (ORFs). Based on sequence similarities to genes in various databases, 2710 ORFs (62.83%) have assigned functions, 1272 ORFs (29.49%) are conserved hypothetical proteins and 331 ORFs (7.67%) are hypothetical proteins (da Silva *et al.*, 2002). Many avirulence/effector protein-coding *Xac* genes have been identified by various functional genomic analyses (Ryan *et al.*, 2011; Brunings & Gabriel, 2003). One of the *Xac* genes involved in citrus canker infection is Xac2369, which encodes a putative general stress protein (XacGSP) consisting of 182 amino-acid residues (Astua-Monge *et al.*, 2005). However, little is known about the biological function of XacGSP. Here, we report the crystal structure of XacGSP determined at 2.5 Å resolution. Structural comparison indicates that XacGSP is structurally similar to pyridoxine 5-phosphate oxidase (PNPOx). Further study confirmed that purified XacGSP binds both flavin mononucleotide (FMN) and flavin adenine dinucleotide (FAD) but has no PNPOx activity.

2. Materials and methods

2.1. Cloning, expression and purification of recombinant XacGSP

XacGSP was cloned from the genomic DNA of *Xac* strain 306 by polymerase chain reaction (PCR) using the forward primer 5'-**GGATCC**ATGGTCAGAGCGAGTTCC-3' and the reverse primer 5'-**GAATTCT**CAGCGCAGCGGAACGTC-3', which were designed based on the nucleotide sequence of the Xac2369 gene (NCBI GeneID 1156440, gi:21243103; da Silva *et al.*, 2002). The oligonucleotide sequences in bold are added sequences corresponding to *Eco*RI and *Hind*III sites, respectively, for cloning purposes. The amplified fragment was first cloned into pMOSBlue vector (pMOSBlue Blunt Ended Cloning Kit, GE Healthcare). Xac2369 DNA was then isolated by double digestion with *Eco*RI–*Hind*III and was subcloned into the *Escherichia coli* expression vector pET-28a (Novagen, Madison, Wisconsin, USA). The resulting plasmid pET28a-XAC2369 expresses XacGSP under the control of the T7 promoter to produce a recombinant protein of 24 kDa consisting of 182 residues of XacGSP plus 36 residues of an N-terminal polyhistidine tag.

Recombinant XacGSP was expressed in *E. coli* strain BL21 (DE3) pLysS cells (Invitrogen, Carlsbad, California, USA). Briefly, a single colony was picked to inoculate a starting culture consisting of 50 ml fresh LB medium (containing 35 µg ml⁻¹ kanamycin and 35 µg ml⁻¹ chloramphenicol) overnight at 310 K and 250 rev min⁻¹. 5 ml of the overnight culture was then inoculated into 2 l fresh LB medium under the same conditions. When the absorbance at 600 nm of the cell culture reached 0.40, incubation was shifted to the lower temperature of 303 K for 20 min at 225 rev min⁻¹. Recombi-

nant protein expression was then induced by the addition of isopropyl β-D-1-thiogalactopyranoside (IPTG) to a final concentration of 0.1 mM. After 4 h of induction, the cells were harvested by centrifugation (5000g, 277 K, 20 min), resuspended in 200 ml lysis buffer (50 mM Tris–HCl pH 8.0, 500 mM NaCl, 60 mM imidazole, 0.5% Nonidet P-40, 5% glycerol, 10 mM benzamidine, 1 mM PMSF) and quickly cooled in liquid nitrogen. Frozen cells were then thawed and disrupted by sonication for 10 min in an ice–water bath. Cell debris was removed by high-speed centrifugation (50 000g for 20 min at 277 K). The clarified supernatant extract was loaded at 3 ml min⁻¹ onto a 5 ml Ni–NTA HisTrap column (GE Healthcare) using an ÄKTApurifier UPC10 (GE Healthcare) at 283 K. After the column had been washed with lysis buffer containing 60 mM imidazole, the bound recombinant protein was eluted with a linear elution gradient of 60–700 mM imidazole. Proteins were monitored by absorbance at 280 nm (*A*₂₈₀) and collected in 3 ml fractions, which were then analyzed by 12% SDS–PAGE. Fractions containing purified XacGSP were pooled and dialyzed against 10 mM Tris–HCl buffer pH 8.0 containing 150 mM NaCl for 12 h at room temperature. Pure XacGSP was concentrated to a final concentration of 15 mg ml⁻¹ using Amicon Ultra filters (30 kDa molecular-weight cutoff; Millipore, Billerica, Massachusetts, USA). 100 µl aliquots were quickly cooled in liquid nitrogen and stored at 193 K for later use.

2.2. Size-exclusion chromatography

The molecular weight of the XacGSP oligomers was determined by size-exclusion chromatography (SEC) on a Sephacryl S-100 High Resolution column (GE Healthcare) equilibrated with 50 mM Tris–HCl buffer pH 8.0 containing 100 mM NaCl. SEC was performed at 283 K with a fraction size of 1 ml and a flow rate of 0.2 ml min⁻¹. The S-100 column was calibrated using a Gel Filtration HMW Calibration Kit (GE Healthcare) including blue dextran 2000, aldolase (158 kDa), conalbumin (75 kDa) and ovalbumin (43 kDa).

2.3. Protein crystallization

All crystallization experiments were carried out at 298 K. Sitting-drop crystallization experiments were carried out using a Phoenix nanodrop crystallization robot (Art Robbins Instruments, Sunnyvale, California, USA) and 96-3 three-well Intelli-Plates to screen initial crystallization conditions against commercial kits including PEG/Ion HT, SaltRx HT, Index HT and PEGRx HT (Hampton Research, Aliso Viejo, California, USA), Wizard Screens I and II (Emerald BioSystems, Bainbridge Island, Washington, USA) and JCSG+ Suite (Qiagen, Valencia, California, USA) screening kits. Drops consisted of equal volumes (200 nl each) of protein solution (15 mg ml⁻¹) and reservoir solution. Plates were stored in a CrystalMation automated protein-crystallization system (Rigaku, USA) and were periodically monitored using a Desktop Minstrel UV automation system (Rigaku, USA). Protein crystals were initially observed in three conditions: (i) 0.1 M sodium acetate buffer pH 4.5, 0.2 M lithium sulfate, 50% PEG 400; (ii) 0.1 M

Table 1

Data-collection and refinement (molecular replacement) statistics.

Values in parentheses are for the highest resolution shell.

Data collection	
X-ray source	SIBYLS, ALS
Wavelength (Å)	1.116
Resolution range (Å)	20.00–2.50 (2.59–2.50)
Space group	$P2_12_12$
No. of images	120
Unit-cell parameters	$a = 120.20$, $b = 122.18$, $c = 57.71$, $\alpha = \beta = \gamma = 90.00$
Completeness (%)	97.0 (98.9)
$R_{\text{merge}}^{\dagger}$ (%)	6.6 (63.9)
Mean $I/\sigma(I)$	22.0 (2.1)
Multiplicity	4.8 (4.6)
Refinement statistics	
Resolution (Å)	20.00–2.50
Total of reflections	29746 (2920)
$R_{\text{work}}/R_{\text{free}}^{\ddagger}$ (%)	0.207/0.239
No. of atoms	
Protein	4263
PEG	20
Water	51
Average B factors (Å ²)	
Protein	58.26
Ligand/ion	38.34
Water	53.14
R.m.s. deviations from ideal geometry	
Bond lengths (Å)	0.006
Bond angles (°)	1.035
Ramachandran plot	
Most favored regions (%)	96.1
Additionally allowed regions (%)	3.9
Generously allowed regions (%)	0.0
Disallowed (%)	0.0
PDB code	3u35

$\dagger R_{\text{merge}} = \sum_{hkl} \sum_i |I_i(hkl) - \langle I(hkl) \rangle| / \sum_{hkl} \sum_i I_i(hkl)$, where $I_i(hkl)$ and $\langle I(hkl) \rangle$ are the observed individual and mean intensities of the reflection with indices hkl , respectively, \sum_i is the sum over i measurements of the reflection with indices hkl and \sum_{hkl} is the sum over all reflections. $\ddagger R = \sum_{hkl} |F_{\text{obs}}| - |F_{\text{calc}}| / \sum_{hkl} |F_{\text{obs}}|$. R_{free} is the R value calculated for 5% of the data set not included in the refinement.

sodium acetate buffer pH 4.5, 1 M (NH₄)₂HPO₄; and (iii) 0.1 M HEPES pH 7.5, 42% PEG 200. After refinement of the crystallization conditions, crystals that were suitable for X-ray data collection were obtained manually by the hanging-drop vapor-diffusion method using 24-well Linbro plates (Hampton Research) containing 500 µl reservoir solution and drops consisting of 2 µl protein solution (15 mg ml⁻¹ in 10 mM Tris–HCl buffer pH 8.0 containing 150 mM NaCl) mixed with 2 µl reservoir solution. XacGSP crystals appeared as single or stacked thin plates with a maximum dimension of 0.20 mm in two weeks at 298 K.

2.4. Data collection and processing

Crystals were first soaked in mother liquor containing up to 45% PEG 200 as a cryoprotectant and then mounted on nylon loops (Hampton Research, Aliso Viejo, California, USA). All crystals were flash-cooled in a liquid-nitrogen stream at 100 K during data collection. Crystals were first evaluated in-house using a Rigaku MicroMax-007 HF X-ray generator (wavelength of 1.541 Å) and a Rigaku R-Axis IV⁺⁺ image-plate detector at UC Riverside. Various crystals were screened and several images per crystal were collected at 100 K using a crystal-to-detector distance of 210 mm. Diffraction images

were collected and indexed with *CrystalClear* v.2.0 (Rigaku) to determine the space group and the diffraction limits of each evaluated crystal. A data set consisting of 200 images at 2.80 Å resolution was collected using this source (PDB entry 3u34). In addition, the best crystals were stored in dewars cooled by liquid nitrogen and shipped to synchrotrons for data collection. A higher resolution data set was collected on the SIBYLS beamline of the Advanced Light Source (Berkeley, California, USA) with a wavelength of 1.116 Å using an ADSC Q315 detector. 120 images were collected using a crystal-to-detector distance of 310 mm, an oscillation width of 1.0° and 5 s exposure time per image. X-ray diffraction intensities were indexed, merged and scaled with *HKL-2000* (Otwinowski & Minor, 1997).

2.5. Structure solution and refinement

The crystal structure of XacGSP was solved by molecular replacement (MR) using the CCP4 program *MOLREP* (Vagin & Teplyakov, 2010; Winn *et al.*, 2011). The putative general stress protein 26 from *X. campestris* pv. *campestris* (PDB entry 3dmb; Joint Center for Structural Genomics, unpublished work) was used as the search model. After MR, cycles of refinement in *PHENIX* (Adams *et al.*, 2010) were alternated with rounds of manual model building in *Coot* (Emsley *et al.*, 2010) using σ_A -weighted ($2F_o - F_c$) and ($F_o - F_c$) electron-density maps. TLS refinement was incorporated into the refinement protocol and the model was divided into different groups according to analysis using the *TLSMD* server (Painter & Merritt, 2006). A total of 5% of reflections were used for R_{free} calculation throughout the refinement process. The final model of the higher resolution (2.50 Å) data set, with an R factor of 20.1% and an R_{free} of 23.9%, contained 607 protein residues, 20 PEG molecules and 51 water molecules. Some residues of the XacGSP protein were not defined in the structural model owing to weak density in the electron-density maps.

2.6. Assays of cofactor binding by XacGSP

Purified XacGSP was incubated in reaction buffer (20 mM Tris–HCl, 100 mM NaCl pH 8.0) with 2 or 3 mM FMN, FAD or PLP for 1 h at room temperature. Excess cofactor was separated from XacGSP by SEC as described in §2.2. The peak fractions of XacGSP were analyzed by UV–Vis spectroscopy in the wavelength range 250–600 nm. Samples of flavin-bound XacGSP (200 µl each) were boiled for 6 min to release flavin, followed by 5 min cooling on ice and 15 min centrifugation (Pédrelacq *et al.*, 2006). The supernatant containing free flavin was analysed by UV–Vis spectroscopy. The concentration of free flavin was calculated using $\epsilon^{446} = 12\,200\text{ M}^{-1}\text{ cm}^{-1}$ for FMN or $\epsilon^{450} = 11\,300\text{ M}^{-1}\text{ cm}^{-1}$ for FAD (Aliverti *et al.*, 1999). The total protein concentration was measured by the Bradford method (Bradford, 1976) using BSA as the standard to estimate the stoichiometric ratio of FMN or FAD and XacGSP monomer (monomer molecular weight = 23 800).

3. Results and discussion

3.1. Crystallization and overall structure of XacGSP

XacGSP was expressed as a recombinant protein fused with an N-terminal His tag, resulting in a calculated molecular weight of 24 kDa. Purified XacGSP was crystallized in several conditions, and the best crystal form was obtained using 0.1 M HEPES buffer pH 7.50 containing 43% PEG 200. X-ray diffraction was observed to 2.80 Å resolution using a rotating-anode X-ray source and to 2.50 Å resolution at a synchrotron. The X-ray diffraction data statistics for the 2.50 Å resolution data are summarized in Table 1. The crystal belonged to space group $P2_12_12$, with unit-cell parameters $a = 120.20$, $b = 122.18$, $c = 57.71$ Å. A BLAST search (Altschul & Lipman, 1990) using the XacGSP polypeptide sequence against the PDB identified a homology structural model (PDB entry 3dmb; Joint Center for Structural Genomics, unpublished work), which was used as the search model for MR (Vagin &

Tepljakov, 2010) to determine the structure of XacGSP. After iterative refinement and model building, the crystallographic R_{work} and R_{free} values of the final XacGSP structural model were 20.1% and 23.9%, respectively (see Table 1). There are four XacGSP molecules in the crystallographic asymmetric unit that form a tetramer consisting of a dimer of dimers ($A-B$ and $C-D$; Fig. 1*a*), in agreement with the estimated Matthews coefficient of $2.16 \text{ Å}^3 \text{ Da}^{-1}$ and solvent content of 43.24% (Matthews, 1968). The first 22 or 23 amino-acid residues at the N-terminus and the last 17 or 18 residues at the C-terminus of the XacGSP subunits are not visible in the electron-density maps, suggesting that these terminal residues are flexible and/or disordered. In addition, partial electron densities were observed for the side chains of residues Lys25, Glu26, Glu29, Lys33, Glu129 and Thr133 in chain *A* (containing residues 24–165); residues Thr24, Lys25, Glu26, Gln28, Lys33, Gln84, Arg86, Glu129 and Glu153 in chain *B* (containing residues 24–164); residues Asp23, Lys25, Glu26, Glu29, Lys33, Gln129, Glu153, Ser154, Ser155, Ile160, Lys161 and Leu163 in chain *C* (containing residues 23–164); and residues Thr24, Lys25, Glu26, Glu29, Gln84, Glu153 and Leu163 in chain *D* (containing residues 24–164). The final structural model of the XacGSP tetramer consists of 607 residues with good geometry: 96.1% are of them in the most favored regions of the Ramachandran plot and 3.9% are in additionally allowed regions, with no residues in disallowed or generously allowed regions (Table 1). The four XacGSP subunits display the same fold (Fig. 1*b*). The root-mean-square deviation is less than 0.5 Å for 142 C α atoms of subunit *A* (cyan) superimposed with subunit *D* (yellow) or for 141 C α atoms of subunit *B* (magenta) superimposed with subunit *C* (green). The root-mean-square deviation increases to about 2 Å for 141 C α atoms of subunit *A* (or *D*) superimposed with subunit *B* (or *C*) because the position of the C-terminal tail (from residue 152 to the C-terminal end) in subunit *A* (or *D*) is different from that in subunit *B* (or *C*).

The monomeric structure of XacGSP contains a β -barrel consisting of six anti-parallel β -strands flanked by five α -helices (Fig. 1*b*): one α -helix (H1) at one end and the four remaining α -helices (H2–H5) at the other end of the barrel. Interestingly, both entrances to the β -barrel are covered by one α -helix and a loop as the 'lid' and 'base': the long α -helix H1 at the N-terminus and the loop connecting strands S2 and S3 form the lid and the short α -helix H2 between strands S3 and S4 together with the loop connecting strands S1 and S2 form the base. A three-helix (H3–H5) bundle connecting strands S4

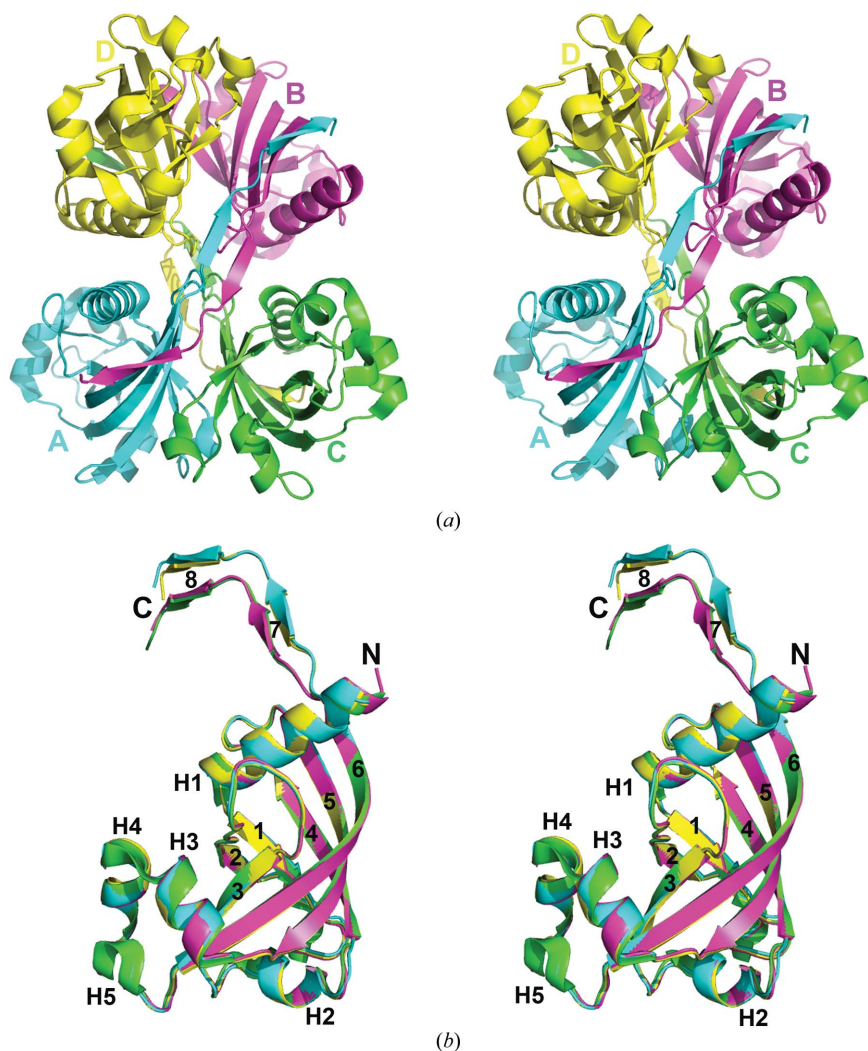


Figure 1

Ribbon representations of the crystal structure of the XacGSP tetramer. (*a*) Stereoview of the XacGSP tetramer observed in the crystal. (*b*) Stereoview of a superimposition of the four XacGSP subunits, which show the same fold but different positions of the C-terminal tail. Structural graphics were prepared with PyMOL (DeLano, 2002). The four monomers *A*, *B*, *C* and *D* are colored cyan, magenta, green and yellow, respectively.

and S5 residues against the outside wall of the β -barrel. In addition, a C-terminal tail extends out from the sixth β -strand (S6) of the barrel. Strand S7 of subunit *A* (or *D*) pairs with its counterpart in subunit *B* (or *C*) to form a 'bridge' (residues 145–164) between the two subunits within the XacGSP dimer (*A*–*B* or *C*–*D*; Fig. 1*a*), while strand S8 of subunit *A* (or *D*) is stabilized by pairing with strand S6 of subunit *B* (or *C*) (Fig. 2). This C-terminal tail provides the major interacting interface for XacGSP dimerization, resulting in a buried surface area of 2910 Å² (calculated by PISA from CCP4; Winn *et al.*, 2011). 15 hydrogen bonds are formed among the main-chain O and N atoms of residues Asp145, Ala147, Ile149, Leu151, Glu153, Ser155, Leu157, Ile160, Val162 and Leu164 of both subunits in the bridge region, which forms the primary interface of the XacGSP dimerization. Two XacGSP dimers cross over each other to form a tetramer in which the β -barrels from one dimer contact the β -barrels of the other dimer and the two dimeric bridges are positioned away from each other without making contacts (Fig. 1*a*). Interestingly, purified XacGSP was observed as dimers and octamers in solution based on analysis by size-exclusion chromatography (SEC). Shown in Fig. 3 are the results of SEC on a Sephacryl S-100 FPLC column

equilibrated with 50 mM Tris–HCl buffer pH 8.0 containing 100 mM NaCl at 283 K. XacGSP eluted in two peaks corresponding to an octamer (with a calculated molecular weight of 192 kDa) and a dimer (with a calculated molecular weight of 48 kDa).

3.2. XacGSP is a flavin-binding protein

Structural and sequence comparisons have provided insight into the biochemical functions and biological roles of hypothetical proteins (Altschul & Lipman, 1990; Pearson, 1998) because of the conservation of structure and function among related proteins (Sander & Schneider, 1991; Koppensteiner *et al.*, 2000). The results of a BLASTP 2.2.25+ sequence-homology search (Altschul *et al.*, 1997) using the National Center for Biotechnology Information (NCBI) website indicate that XacGSP shares high sequence homology with putative general stress proteins from the genus *Xanthomonas*, but no homologous proteins with known biological functions were identified. A search for structurally related proteins was performed using the DALI server (Holm *et al.*, 2008) and several structural homologs ($Z > 8$) were identified (Table 2). Apart from a putative general stress protein 26 from *X. campestris*, in agreement with the results of the BLASTP search, these proteins with known structures have low amino-acid sequence identity (10–29%) to XacGSP. All of these proteins are flavin-binding proteins and most of them are PNPOx enzymes. PNPOx uses FMN as a cofactor and catalyses the final step in biosynthesis of pyridoxal 5'-phosphate (PLP), a cofactor used by various enzymes involved in amino-

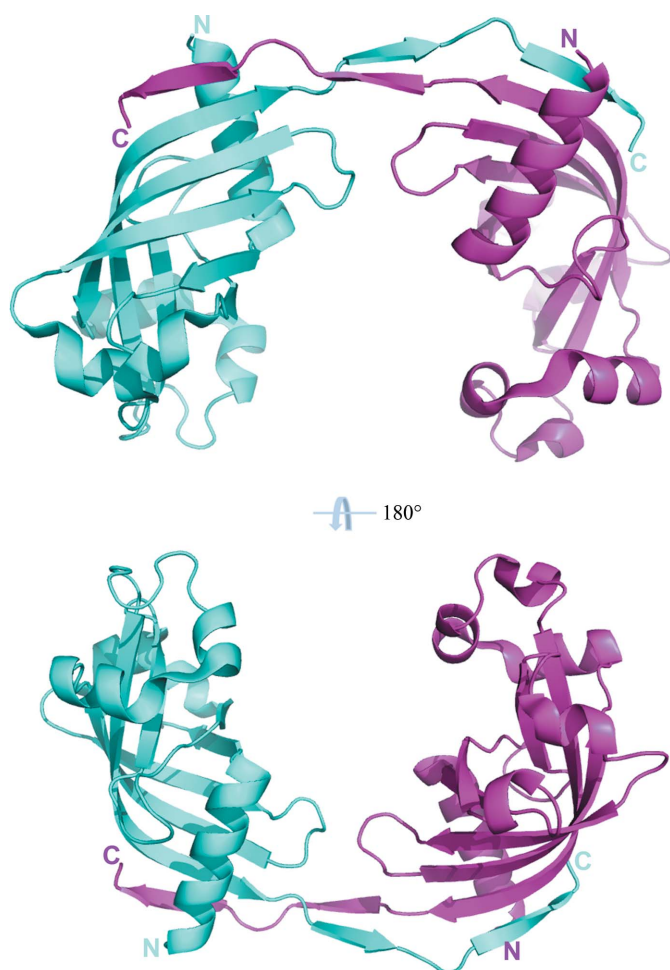


Figure 2

Ribbon representations of the XacGSP dimer structure. The two monomers (*A* and *B*) are colored cyan and magenta, respectively.

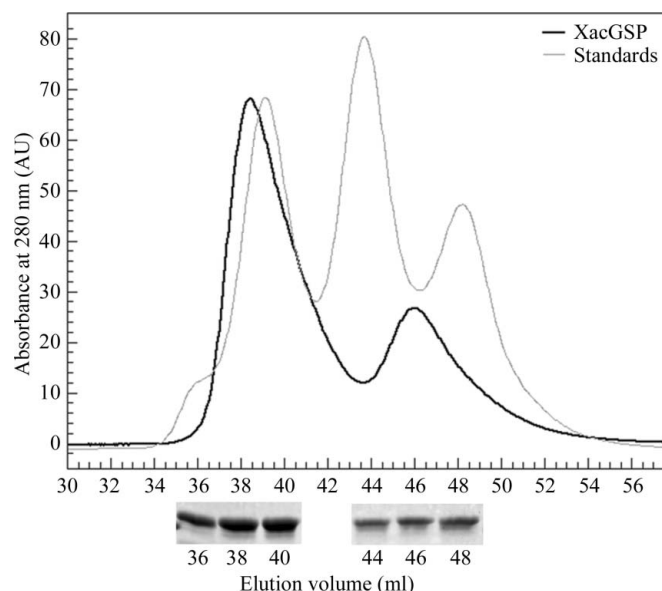


Figure 3

Results of size-exclusion chromatography of XacGSP. A chromatogram of the eluted fractions is shown. XacGSP was loaded onto a Sephacryl S-100 HR size-exclusion column. The peaks represent the absorbance of proteins at 280 nm. The column was calibrated with aldolase (158 kDa), conalbumin (75 kDa) and ovalbumin (43 kDa) standards in a separate experiment. 12% SDS–PAGE analysis of the peak fractions collected during size-exclusion chromatography is shown below the chromatogram. The fraction size was 1 ml per tube at a flow rate of 0.2 ml min^{−1}.

Table 2XacGSP structural homologs identified by the DALI server (Holm *et al.*, 2008).

Protein	Size†	Organism	Sequence identity (%)	Z score	R.m.s.d. (Å)	PDB entry	Ligand	Reference‡
Putative general stress protein 26	147	<i>Xanthomonas campestris</i>	94.0	22.9	2.6	3dmb	—	Joint Center for Structural Genomics
Putative general stress protein 26	160	<i>Jannaschia</i> sp.	29.0	15.9	3.5	2qea	—	Joint Center for Structural Genomics
Pyridoxamine 5'-phosphate oxidase-related protein	134	<i>Psychrobacter arcticus</i>	25.0	15.5	2.1	2re7	—	Joint Center for Structural Genomics
Pyridoxine 5'-phosphate oxidase	148	<i>Nostoc punctiforme</i>	22.0	14.4	2.4	2i02	FMN	Joint Center for Structural Genomics
Putative general stress protein 26	139	<i>Bacillus anthracis</i>	18.0	14.4	2.1	3ec6	FAD	Center for Structural Genomics of Infectious Diseases
General stress protein 26	141	<i>Bacillus thtaiotaomicron</i>	23.0	14.3	2.2	2fhq	—	Midwest Center for Structural Genomics
Putative pyridoxamine 5'-phosphate oxidase	128	<i>Listeria innocua</i>	18.0	13.5	2.7	3db0	—	Joint Center for Structural Genomics
General stress protein 26	146	<i>Clostridium acetobutylicum</i>	15.0	13.5	2.5	2hq7	—	Joint Center for Structural Genomics
FAD-binding protein	149	<i>Mesorhizobium loti</i>	15.0	12.0	2.6	2hq9	FAD	Joint Center for Structural Genomics
Flavin nucleotide-binding protein	185	<i>Bacillus halodurans</i>	15.0	11.9	2.6	2hti	FAD	Joint Center for Structural Genomics
Uncharacterized protein	148	<i>Corynebacterium diphtheriae</i>	12.0	11.4	2.6	3cp3	—	Midwest Center for Structural Genomics
PAI 2 protein	202	<i>Bacillus stearothermophilus</i>	7.0	11.4	2.8	2ol5	—	Filippova <i>et al.</i> (2011)
Hypothetical protein Rv1155	147	<i>Mycobacterium tuberculosis</i>	11.0	11.3	2.9	1w9a	—	Canaan <i>et al.</i> (2005)
Pyridoxine 5'-phosphate oxidase	147	<i>Mycobacterium tuberculosis</i>	11.0	11.3	3.0	2aq6	PLP	Biswal <i>et al.</i> (2005)
Uncharacterized protein Atu2129	258	<i>Agrobacterium tumefaciens</i>	19.0	11.2	2.8	3dnh	—	Midwest Center for Structural Genomics
Putative pyridoxamine 5'-phosphate oxidase	138	<i>Corynebacterium glutamicum</i>	11.0	11.1	2.7	3fkh	—	Joint Center for Structural Genomics
Hypothetical protein	209	<i>Thermoplasma acidophilum</i>	14.0	10.9	4.0	2fur	—	Joint Center for Structural Genomics
Protein with FMN-binding split-barrel fold	155	<i>Streptomyces avermitilis</i>	13.0	10.8	2.7	2iab	—	Joint Center for Structural Genomics
NimC/NimA-family protein	150	<i>Clostridium acetobutylicum</i>	13.0	10.7	2.8	2ig6	FMN	Joint Center for Structural Genomics
Hypothetical protein Rv2074	137	<i>Mycobacterium tuberculosis</i>	9.0	10.7	2.7	2asf	—	Biswal <i>et al.</i> (2006)
Pyridoxine 5'-phosphate oxidase	145	<i>Lactobacillus plantarum</i>	7.0	10.7	3.2	3ba3	—	Joint Center for Structural Genomics
Cellular repressor of E1A-stimulated genes	184	<i>Homo sapiens</i>	12.0	10.5	3.1	1xhn	—	Sacher <i>et al.</i> (2005)
Pyridoxamine 5'-phosphate oxidase-related protein	195	<i>Nostoc</i> sp.	14.0	10.4	3.0	2i51	FMN	Joint Center for Structural Genomics
Pyridoxine 5'-phosphate oxidase	175	<i>Jannaschia</i> sp.	13.0	10.1	3.6	2ou5	FMN	Joint Center for Structural Genomics
Putative 5-nitroimidazole antibiotic-resistance protein	178	<i>Bacteroides thtaiotaomicron</i>	12.0	10.1	3.3	2fg9	FAD	Joint Center for Structural Genomics
Pyridoxine 5'-phosphate oxidase	150	<i>Streptococcus suis</i>	17.0	10.0	3.3	2hhz	—	Joint Center for Structural Genomics
Heme oxygenase	259	<i>Helicobacter pylori</i>	12.0	10.0	5.3	3gas	—	F. Jiang, Y.-L. Hu, Y. Guo, G. Guo, Q.-M. Zou & D.-C. Wang
FMN-binding protein	122	<i>Desulfovibrio vulgaris</i>	20.0	9.8	2.8	1flm	FNM	Suto <i>et al.</i> (2000)
Predicted flavin nucleotide-binding protein	140	<i>Lactobacillus delbrueckii</i>	9.0	9.4	2.6	2htd	—	Joint Center for Structural Genomics
Pyridoxine 5'-phosphate oxidase	199	<i>Escherichia coli</i>	11.0	9.2	3.2	1dnl	FMN	Safo <i>et al.</i> (2000)
5-Nitroimidazole antibiotic-resistance-related protein	216	<i>Deinococcus radiodurans</i>	13.0	9.1	4.3	1w3p	—	Leiros <i>et al.</i> (2004)
Pyridoxine 5'-phosphate oxidase	246	<i>Mycobacterium tuberculosis</i>	14.0	8.9	3.1	2a2j	—	Pédelaq <i>et al.</i> (2006)
Uncharacterized protein	151	<i>Exiguobacterium sibiricum</i>	17.0	8.5	2.9	2q9k	—	Joint Center for Structural Genomics
Probable pyridoxine 5'-phosphate oxidase	214	<i>Pseudomonas aeruginosa</i>	16.0	8.5	3.4	1t9m	FMN	Parsons <i>et al.</i> (2004)
FMN-binding protein	148	<i>Syntrophomonas wolfei</i>	11.0	8.4	2.8	3in6	FMN	Joint Center for Structural Genomics
Pyridoxine 5'-phosphate oxidase R229W mutant	261	<i>Homo sapiens</i>	11.0	8.4	3.4	3hy8	FMN, PLP	Musayev <i>et al.</i> (2009)
Pyridoxine 5'-phosphate oxidase	261	<i>Homo sapiens</i>	10.0	8.3	3.5	1nrg	FMN, PLP	Musayev <i>et al.</i> (2003)
Pyridoxine 5'-phosphate oxidase	228	<i>Saccharomyces cerevisiae</i>	9.0	8.3	3.4	1ci0	FMN	New York SGX Research Center for Structural Genomics

† Protein sizes are expressed as number of amino-acid residues. ‡ Where no year of publication is given, the work is unpublished.

acid metabolism (Zhao *et al.*, 1995; Safo *et al.*, 2000, 2001; di Salvo *et al.*, 2002, 2003; Musayev *et al.*, 2003).

The structural similarity of XacGSP to these FMN-binding proteins suggests that XacGSP should bind to FMN and/or FAD. To test this, we incubated XacGSP with 2 mM FMN or FAD and separated the protein from free FMN or FAD by size-exclusion chromatography. The XacGSP eluted from the SEC column was yellow, which is an indication of an FMN- or FAD-bound protein. The binding of FMN or FAD by XacGSP

was further analyzed by UV-Vis spectroscopy. As shown in Fig. 4, binding of FMN or FAD by XacGSP shows absorbance at 385 and 465 nm, while apo XacGSP has no absorbance at these two wavelengths. When these FMN- or FAD-bound XacGSP samples were denatured by NaOH to release the cofactor, the released free FMN or FAD shows a shift of 15–20 nm to the shorter wavelength at the absorbance peak (Figs. 4*a* and 4*b*). Based on $\epsilon^{446} = 12\,200\text{ M}^{-1}\text{ cm}^{-1}$ for FMN or $\epsilon^{450} = 11\,300\text{ M}^{-1}\text{ cm}^{-1}$ for FAD (Aliverti *et al.*, 1999),

XacGSP binds one FMN or FAD per monomer. However, when PLP was tested the UV–Vis spectra were the same for XacGSP with PLP as for apo XacGSP (Fig. 4c), indicating that XacGSP does not bind PLP. PLP is the product of the reaction mediated by PNPOx and has been shown to bind tightly to the PNPOx enzyme (Musayev *et al.*, 2003; Safo *et al.*, 2001; Yang & Schirch, 2000; Zhao & Winkler, 1995). Therefore, we believe that XacGSP is not a PNPOx enzyme but an FMN- or FAD-binding protein probably involved in resistance to oxidative stresses induced by the defense responses of the plant.

Our observation that XacGSP binds to FMN (or FAD) but not to PLP is consistent with the crystal structure of XacGSP. When the structure of the XacGSP monomer is superimposed with that of *E. coli* PNPOx associated with PLP and FMN (PDB entry 1g76; Safo *et al.*, 2001), XacGSP has an FMN-binding pocket similar to that observed in PNPOx (Fig. 5). The three positively charged residues Arg67, Arg88 and Lys89 in PNPOx that interact with the phosphate group of FMN are

partially conserved as Arg54, Ala77 and Ala78 in XacGSP. However, this binding pocket is smaller in XacGSP and cannot hold both FMN and PLP, explaining why XacGSP does not bind to PLP. However, the aromatic ring of Trp127 is likely to function in the same way as the pyridine ring of PLP in PNPOx to stack with the isoalloxazine ring of FMN (Fig. 5). In addition, the two positively charged residues Arg133 and Lys72 that interact with the phosphate group of PLP in PNPOx are also missing in XacGSP: the corresponding position of Lys72 in PNPOx is occupied by the negatively charged residue Glu59, while the whole α -helix corresponding to the α -helix containing Arg133 in PNPOx is shifted, with the corresponding position occupied by the hydrophobic residue Tyr122 (or Val123) in XacGSP (Fig. 5). However, the FMN-bound XacGSP has to position FMN higher in the binding pocket to avoid a clash with residue Arg54. Interestingly, the helix–turn–helix motif over the active site in PNPOx is missing in XacGSP, leaving the flavin-binding pocket open to the solvent environment (Fig. 5); this is not conducive to the oxidative reaction mediated by PNPOx enzymes and explains why XacGSP is not a PNPOx enzyme. In addition, the open flavin-binding pocket provides an open space for the adenine ribonucleotide of FAD, allowing XacGSP to also bind FAD. Because both FMN and FAD are redox factors for many proteins, we speculate that XacGSP is involved in providing resistance to oxidative stresses induced by the defense responses of the plant. The flavin-binding pocket on the surface of XacGSP may facilitate this function. Attempts to cocrystallize XacGSP with FMN (or FAD) are being made. Currently, the biological function of XacGSP remains elusive, although functional genetic analysis indicated that XacGSP plays a role in citrus infection. The results presented in this paper are an important first step in unravelling the biological function of XacGSP at the molecular level.

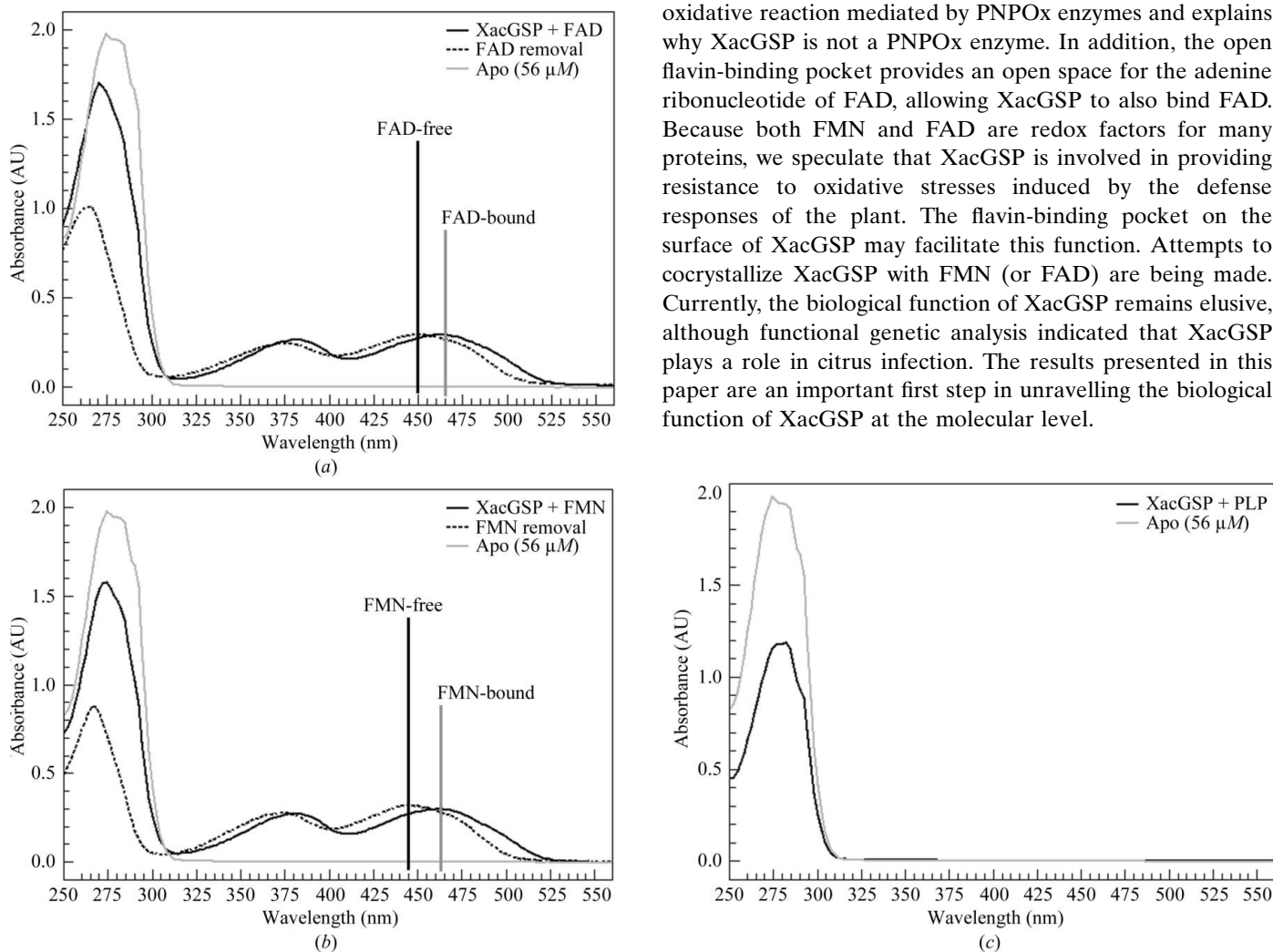


Figure 4

UV–Vis spectra of XacGSP and its interactions with FAD (a), FMN (b) and PLP (c). In all plots, the spectrum of XacGSP free of cofactors (apo) is shown as a light gray line. FAD- or FMN-bound XacGSP was prepared by incubation of XacGSP with the cofactor and was followed by purification by SEC. The spectra (XacGSP + FAD or XacGSP + FMN) are shown as solid black lines. FMN or FAD was then released by denaturing the cofactor-bound protein sample and centrifugation. The spectra of the released cofactors (FMN removal or FAD removal) are shown as dashed black lines. The characteristic peaks of free FMN or FAD and FMN-bound or FAD-bound XacGSP are indicated.

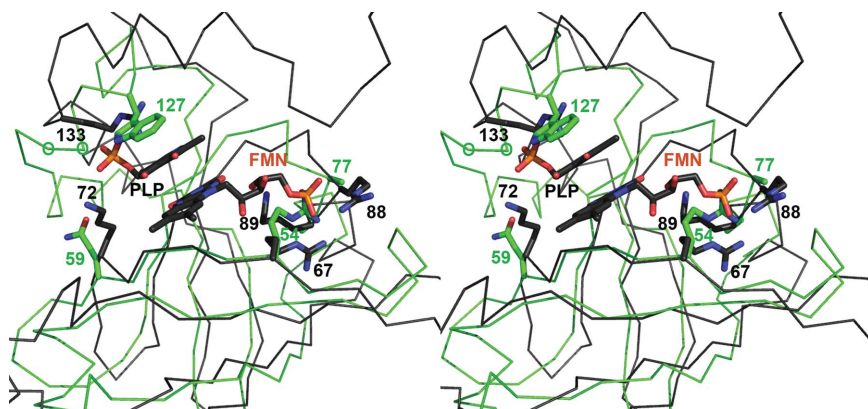


Figure 5

Stereoview of the FMN-binding pockets of XacGSP and *E. coli* PNPOx. The backbone structure of the XacGSP monomer (green wires) was superimposed with that of *E. coli* PNPOx (black wires) in complex with PLP and FMN (PDB entry 1g76). The side chains of residues Arg54, Glu59, Ala77, Ala78 and Trp127 in XacGSP are shown as green sticks, while the side chains of residues Arg67, Lys72, Arg88, Lys89 and Arg133 as well as PLP and FMN in PNPOx are shown as black sticks. The C α positions of residues Tyr122 and Val123 in XacGSP are indicated by small green circles. The O, N and P atoms of the side chains are shown in red, blue and orange, respectively.

This work was funded by UC-Riverside (to LF). We would like to acknowledge the staff at the SIBYLS beamline of the Advanced Light Source (ALS; Berkeley, California, USA). EH would like to thank Maria Célia Bertolini at Departamento de Bioquímica e Tecnologia Química, Instituto de Química, UNESP, Araraquara-SP, Brazil.

References

- Adams, P. D. *et al.* (2010). *Acta Cryst.* **D66**, 213–221.
- Aliverti, A., Curti, B. & Vanoni, M. A. (1999). *Methods Mol. Biol.* **131**, 9–23.
- Altschul, S. F. & Lipman, D. J. (1990). *Proc. Natl Acad. Sci. USA*, **87**, 5509–5513.
- Altschul, S. F., Madden, T. L., Schäffer, A. A., Zhang, J., Zhang, Z., Miller, W. & Lipman, D. J. (1997). *Nucleic Acids Res.* **25**, 3389–3402.
- Astua-Monge, G., Freitas-Astua, J., Bacocina, G., Roncoletta, J., Carvalho, S. A. & Machado, M. A. (2005). *J. Bacteriol.* **187**, 1201–1205.
- Biswal, B. K., Au, K., Cherney, M. M., Garen, C. & James, M. N. G. (2006). *Acta Cryst.* **F62**, 735–742.
- Biswal, B. K., Cherney, M. M., Wang, M., Garen, C. & James, M. N. G. (2005). *Acta Cryst.* **D61**, 1492–1499.
- Bradford, M. M. (1976). *Anal. Biochem.* **72**, 248–254.
- Brunings, A. M. & Gabriel, D. W. (2003). *Mol. Plant Pathol.* **4**, 141–157.
- Canaan, S., Sulzenbacher, G., Roig-Zamboni, V., Scappuccini-Calvo, L., Frassinetti, F., Maurin, D., Cambillau, C. & Bourne, Y. (2005). *FEBS Lett.* **579**, 215–221.
- Civerolo, E. L. (1984). *J. Rio Grande Valley Hort. Soc.* **37**, 127–145.
- Cubero, J., Graham, J. H. & Gottwald, T. R. (2001). *Appl. Environ. Microbiol.* **67**, 2849–2852.
- da Silva, A. C. *et al.* (2002). *Nature (London)*, **417**, 459–463.
- DeLano, W. L. (2002). *PyMOL*. <http://www.pymol.org>.
- Matthews, B. W. (1968). *J. Mol. Biol.* **33**, 491–497.
- Musayev, F. N., Di Salvo, M. L., Ko, T.-P., Schirch, V. & Safo, M. K. (2003). *Protein Sci.* **12**, 1455–1463.
- Musayev, F. N., di Salvo, M. L., Saavedra, M. A., Contestabile, R., Ghatge, M. S., Haynes, A., Schirch, V. & Safo, M. K. (2009). *J. Biol. Chem.* **284**, 30949–30956.
- Otwinowski, Z. & Minor, W. (1997). *Methods Enzymol.* **276**, 307–326.
- Painter, J. & Merritt, E. A. (2006). *Acta Cryst.* **D62**, 439–450.
- Parsons, J. F., Calabrese, K., Eisenstein, E. & Ladner, J. E. (2004). *Acta Cryst.* **D60**, 2110–2113.
- Pearson, W. R. (1998). *J. Mol. Biol.* **276**, 71–84.
- Pédélecq, J.-D., Rho, B.-S., Kim, C.-Y., Waldo, G. S., Lakin, T. P., Segelke, B. W., Rupp, B., Hung, L.-W., Kim, S.-I. & Terwilliger, T. C. (2006). *Proteins*, **62**, 563–569.
- Ryan, R. P., Vorhölter, F. J., Potnis, N., Jones, J. B., Van Sluys, M. A., Bogdanove, A. J. & Dow, J. M. (2011). *Nature Rev. Microbiol.* **9**, 344–355.
- Sacher, M., Di Bacco, A., Lunin, V. V., Ye, Z., Wagner, J., Gill, G. & Cygler, M. (2005). *Proc. Natl Acad. Sci. USA*, **102**, 18326–18331.
- Safo, M. K., Mathews, I., Musayev, F. N., di Salvo, M. L., Thiel, D. J., Abraham, D. J. & Schirch, V. (2000). *Struct. Fold. Des.* **8**, 751–762.
- Safo, M. K., Musayev, F. N., di Salvo, M. L. & Schirch, V. (2001). *J. Mol. Biol.* **310**, 817–826.
- Sander, C. & Schneider, R. (1991). *Proteins*, **9**, 56–68.
- Suto, K., Kawagoe, K., Shibata, N., Morimoto, Y., Higuchi, Y., Kitamura, M., Nakaya, T. & Yasuoka, N. (2000). *Acta Cryst.* **D56**, 368–371.
- Vagin, A. & Teplyakov, A. (2010). *Acta Cryst.* **D66**, 22–25.
- Winn, M. D. *et al.* (2011). *Acta Cryst.* **D67**, 235–242.
- Yang, E. S. & Schirch, V. (2000). *Arch. Biochem. Biophys.* **377**, 109–114.
- Zhao, G., Pease, A. J., Bharani, N. & Winkler, M. E. (1995). *J. Bacteriol.* **177**, 2804–2812.
- Zhao, G. & Winkler, M. E. (1995). *J. Bacteriol.* **177**, 883–891.
- di Salvo, M. L., Ko, T.-P., Musayev, F. N., Raboni, S., Schirch, V. & Safo, M. K. (2002). *J. Mol. Biol.* **315**, 385–397.
- di Salvo, M. L., Safo, M. K., Musayev, F. N., Bossa, F. & Schirch, V. (2003). *Biochim. Biophys. Acta*, **1647**, 76–82.
- Emsley, P., Lohkamp, B., Scott, W. G. & Cowtan, K. (2010). *Acta Cryst.* **D66**, 486–501.
- Filippova, E. V., Brunzelle, J. S., Cuff, M. E., Li, H., Joachimiak, A. & Anderson, W. F. (2011). *Proteins*, **79**, 2578–2582.
- Graham, J. H., Gottwald, T. R., Cubero, J. & Achor, D. S. (2004). *Mol. Plant Pathol.* **5**, 1–15.
- Holm, L., Kääriäinen, S., Rosenström, P. & Schenkel, A. (2008). *Bioinformatics*, **24**, 2780–2781.
- Koppensteiner, W. A., Lackner, P., Wiederstein, M. & Sippl, M. J. (2000). *J. Mol. Biol.* **296**, 1139–1152.
- Laia, M. L., Moreira, L. M., Dezajacomo, J., Brigati, J. B., Ferreira, C. B., Ferro, M. I., Silva, A. C., Ferro, J. A. & Oliveira, J. C. (2009). *BMC Microbiol.* **9**, 12.
- Leiros, H.-K. S., Kozielski-Stuhmann, S., Kapp, U., Terradot, L., Leonard, G. A. & McSweeney, S. M. (2004). *J. Biol. Chem.* **279**, 55840–55849.